Int. J. Electrochem. Sci., 12 **(2017)** 11754 – 11762, doi: 10.20964/2017.12.19

International Journal of
ELECTROCHEMICAL
SCIENCE
www.electrochemsci.org

Facile Synthesis of $NH_4V_3O_8$ Micro/Nanoplates and the Effects of Cutoff Potential on Electrochemical Performance

Liang Liu[*], *Qiang Liu, Wen Zhao, Limei Wang, Guochun Li, Long Chen*

Automotive Engineering Research Institute, Jiangsu University, Zhenjiang 212013, China
[*]E-mail: lliu@ujs.edu.cn

Received: 31 August 2017 / *Accepted:* 19 October 2017 / *Published:* 12 November 2017

$NH_4V_3O_8$ micro/nanoplates are synthesized using a hydrothermal method without any surfactant. The $NH_4V_3O_8$ micro/nanoplate cathodes show a high initial discharge capacity of 406 mAh g^{-1}, owing to the unique microscopic crystal structure and macroscopic 2D architectures, which enlarge the contacted area with the electrolyte solution. It is found that the voltage cutoff plays an important role in the capacity and cyclability. The lithium ion insertion site at 1.8 V causes the layered structure disorder/destruction, resulting in strong polarization and amorphization. In the suitable potential of 2-4 V, the reaction kinetics in $NH_4V_3O_8$ electrodes are not altered upon cycling, exhibiting improved cyclability and a high performance rate for lithium ion batteries.

Keywords: Ammonium trivanadate; Micro/nanoplates; Lithium ion battery; Cathode materials; Cutoff potentials

1. INTRODUCTION

Lithium ion batteries (LIBs) have attracted great interest as power sources for hybrid electric vehicles (HEVs) or electric vehicles (EVs) because of their light weight and high power density[1]. To meet the demands of energy density and cycle life for LIBs, the design and fabrication of effective electrode structures, especially cathode materials, is essential. This improved design will be a remarkable progression for high performance LIBs[2]. Among them, vanadium oxides, such as VO_2 and V_2O_5 have been evaluated as promising candidates due to their high theoretical capacity, low cost and ease of synthesis[3-6]. However, the irreversible phase transformation or even amorphization during the lithiation and delithiation process could lead to the collapse of the crystal's layered structure and short cycle life[7].

In comparison to vanadium oxides, vanadium bronzes with mixed valent network $[V_xO_y]$ containing the V-V couples have more stable crystal structures. The cations between the $[V_xO_y]$ layers would stabilize the crystal structures, increase the electrical conductivity and the diffusion rate of lithium ions[8]. Ammonium trivanadate as a representative of the vanadium bronzes has attractive electrochemical characteristics[9]. It consists of VO_5 square pyramids and VO_6 octahedrons with NH_4^+ cations between the vanadium-oxide layers. As expected, the V–O framework combined with favourable connectivity between the vanadium centres render this material a good electrical conduit and provides a pathway for the diffusion of lithium ions. Due to the relatively stable layered structure, $NH_4V_3O_8$ exhibits a great potential to be used as cathode materials for high-power and long-cycling life LIBs[10]. Various structures of ammonium vanadate and their derivative have been developed, such as $NH_4V_3O_8{\cdot}0.37H_2O$ nanorods[11], $NH_4V_3O_8{\cdot}0.2H_2O$ flakes[12], $NH_4V_3O_8$ nanobelts[13] and $NH_4V_4O_{10}$ nanowire flowers[14]. However, the nanosized particles can easily aggregate owing to their high surface energy, which will severely limit their effectiveness, as well as their usefulness in industrial applications[15]. Inspired by the superiority of structures[16, 17], we demonstrate $NH_4V_3O_8$ micro/nanoplates composed of high crystallined nanosheets by a facile hydrothermal synthesis. The structures can ensure the high surface area contact with electrolytes and exhibit high discharge capacities. To avoid the irreversible phase transformation and amorphization, the effects of cutoff potentials (1.5-4 V vs. 2-4 V) have been investigated. It is found that the cutoff potentials have great influence on the stability of the crystal structures. The $NH_4V_3O_8$ micro/nanoplates cathodes exhibit better cycling stability and rate capability in 2 V cutoff potentials than that in 1.5 V, owing to their fast kinetics for Li ions and decreased polarization during the lithiation/delithiation process.

2. EXPERIMENTAL SECTION

2.1 Synthesis of $NH_4V_3O_8$ micro/nanoplates

All chemical reagents (analytical grade purity) are purchased from Shanghai Chemical Company and used without any further purification. In a typical synthesis, 1 mmol of NH_4VO_3 are dissolved in 30 mL of deionized water. Then 1.5 mmol benzoic acid is added into the solution and stirred for 12 hours. Subsequently, the resulting solution is transferred into a 60 mL Teflon-lined autoclave. The autoclave is sealed, maintained at 180°C for 48 h and cooled to room temperature naturally. The precipitate is collected and washed for several times with distilled water and absolute ethanol, respectively. Finally, the products are dried in a vacuum at 60 °C for 6 h.

2.2 Sample Characterization

The crystalline structure of the samples is characterized by X-ray powder diffraction (XRD) with a Japan Rigaku D/max rA X-ray diffractometer. The field emission scanning electron microscopy (SEM) images are taken on a FEI Sirion-200 SEM. The transmission electron microscopy (TEM) images are performed with a Hitachi Model H-800 instrument. High-resolution transmission electron microscopy (HRTEM) images and electron diffraction (ED) patterns are carried out on a JEOL-2010

TEM. The thermogravimetric (TG) analysis of the as-synthesized samples were carried out on SDT Q600 (V20.9 Build 20) at a heating rate of 10 °C min^{-1} from room temperature to 600 °C.

2.3 Electrochemical measurement

The positive electrodes are fabricated by mixing as-prepared $NH_4V_3O_8$ micro/nanoplates, acetylene black and polytetrafluorethylene (PTFE) in a weight ratio of 75:15:10 with ethanol as dispersant. The paste is compressed into a thin piece with a roller. The obtained piece is cut into a disk film of 8 mm in diameter, which is dried at 80 °C for 12 h in vacuum oven. The average mass loading amount of the active materials are 5.8 mg cm^{-2}. To test battery performance, the half-cells are assembled of working electrodes, a microporous polypropylene film, and metallic lithium as anode and 1 M $LiPF_6$ in 1:1:1 EC/DMC/EMC electrolyte. Galvanostatic discharge/charge cycling tests are carried out at ambient temperature using the LANDCT2001A (Wuhan Jinnuo, China). The electrochemical impedance spectroscopy (EIS) measurement is conducted using the Zahner Zennium E electrochemical workstation in the frequency range of 100 kHz - 10 mHz, while the disturbance amplitude is 5 mV.

3. RESULTS AND DISCUSSION

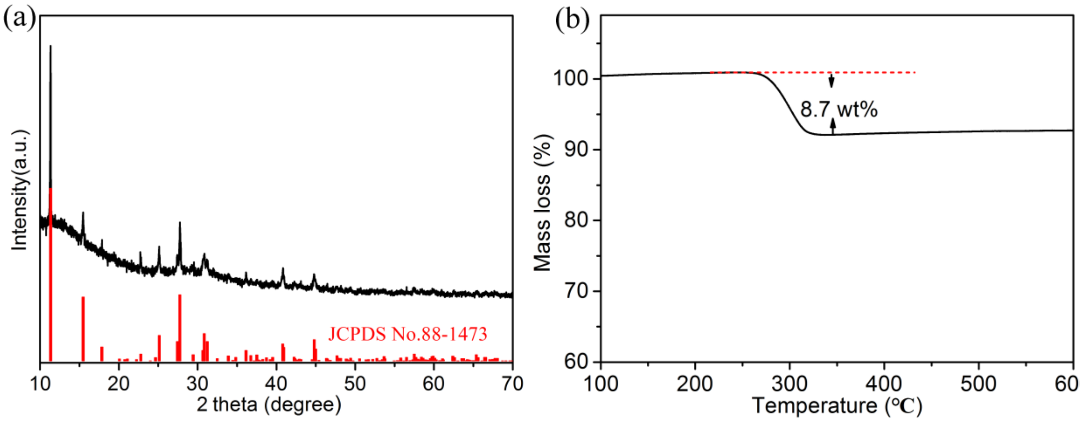

Figure 1. (a) XRD patterns (b) TG curve and of the $NH_4V_3O_8$ samples.

The preliminary analysis of the phase and purity is studied by X-ray powder diffraction pattern (XRD). Fig. 1a shows a typical XRD patterns of the as-prepared $NH_4V_3O_8$ samples, which could be readily indexed to monoclinic phase $NH_4V_3O_8$ (JCPDS No.88-1473). No obvious peaks of other phases are detected, indicating high purity and good crystallinity of ammonium trivanadate. The thermogravimetric (TG) analysis further characterize the heating-treatment process, which attributed to the decomposition of ammonium trivandate, shown as the following Eq. (1):

$$2NH_4V_3O_8 \rightarrow 3V_2O_5 + 2NH_3\uparrow + H_2O\uparrow \qquad (1)$$

As shown in Fig. 1b, an obvious mass loss of 8.7 wt % between 250-330 °C is in good agreement with the theoretical value of the weight loss according to the Eq. (1). It further demonstrates that its structure phase is the pure $NH_4V_3O_8$ with no water of hydration, which is different from the samples synthesized under the help of surfactant in previous report[12].

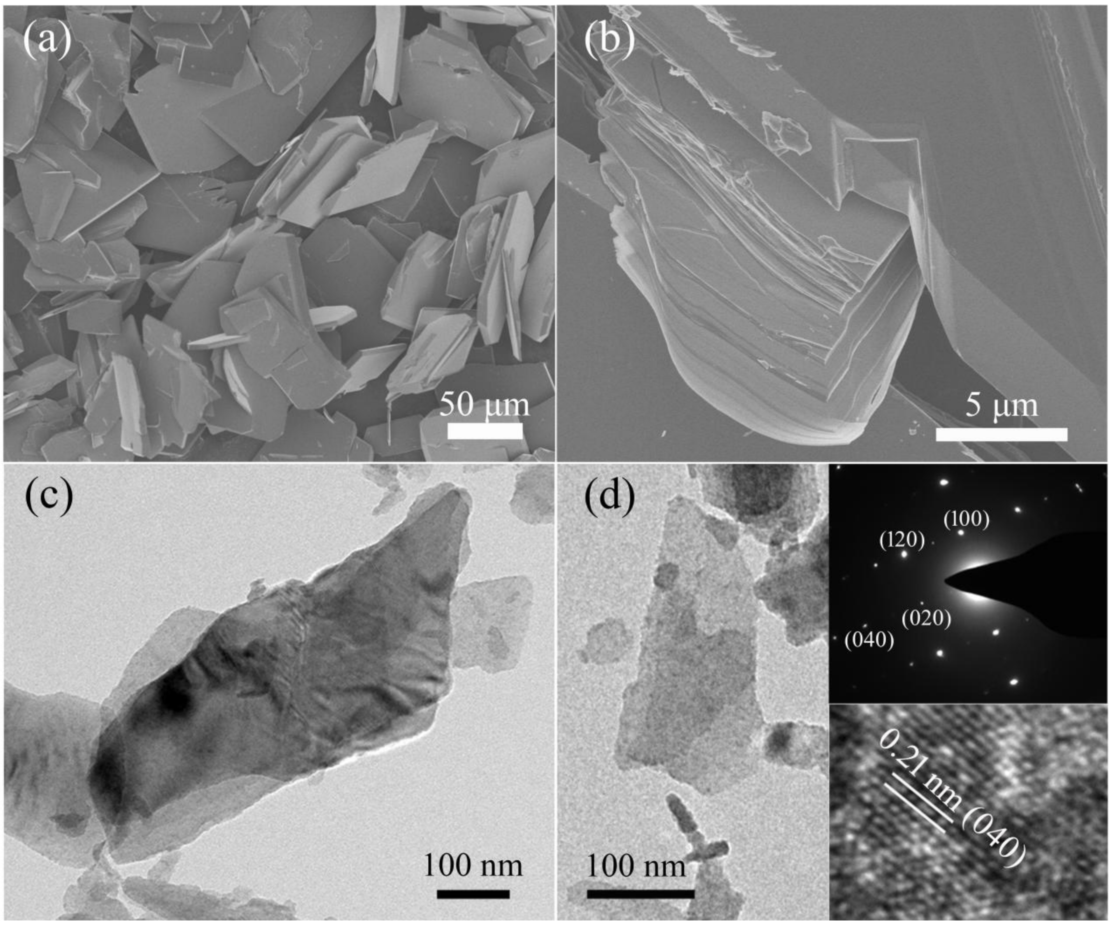

Figure 2. (a) SEM image of the $NH_4V_3O_8$ microplates. (b) Enlarged SEM image on the edge of the $NH_4V_3O_8$ microplate. (c) TEM image of ultrasonically exfoliated $NH_4V_3O_8$ nanosheets from the as-prepared $NH_4V_3O_8$ microplates. (d) TEM and HRTEM image of an individual nanosheet and corresponding SAED pattern.

The morphology of the as-prepared $NH_4V_3O_8$ samples is examined by field emission scanning electron microscopy (SEM). As shown in Fig. 2a, the SEM image revealed that the single microplate size is up to 80 μm. From the enlarged SEM image (Fig. 2b), layers of assembled nanosheets could be seen on the edge of the $NH_4V_3O_8$ microplate. The careful observation can be found that such an integral microplate is actually made up of layered structures. The transmission electron microscopic (TEM) image (Fig. 2c) clearly exhibit the nanosheets ultrasonically exfoliated from the layered structures of the $NH_4V_3O_8$ microplates. The lateral size of the nanosheet is approximately 600 nm. Further observation of the individual nanosheet revealed by high-magnified TEM image (Fig. 2d) shows their large-area sheet-like morphology. The spotty rings in the selected-area electron diffraction

(SAED) (Fig. 2d top insert) show the single crystallined nature of the ultrasonically exfoliated individual nanosheet. The diffraction pattern of (020), (120) and (100) can also be seen. The associated high-resolution transmission electron microscopy (HRTEM) (Fig. 2d lower insert) show the lattice spacing of 0.21 nm which corresponds to the separations between (040) planes.

In the synthesis process, benzoic acid in the solution provided an acidic environment, which impacted the crystallite morphology. The basic reaction for the synthesis of ammonium trivanadate microcrystals can be formally formulated as the follows Eq. (2):

$$3NH_4VO_3 + C_6H_5COOH \rightleftharpoons NH_4V_3O_8 + C_6H_5COONH_4 + NH_3 + H_2O \quad (2)$$

In detail, when benzoic acid is added in water, the previous dissolved hydrolyzed vanadium precursor, vanadium polyanions, are surrounded by dipolar water molecules giving $[VO(OH)_2(OH_2)_3]^+$ solvated species[18]. The condensation occurs predominantly *via* olation along the H_2O–V–OH directions. Both x and y directions are equivalent regarding condensation, while there is no condensation reaction in the *z* direction due to the absence of V–OH in the H_2O–V=O groups. As a result, two dimensional $NH_4V_3O_8$ crystallites (nanosheets) are formed within the *xy* plane[19].

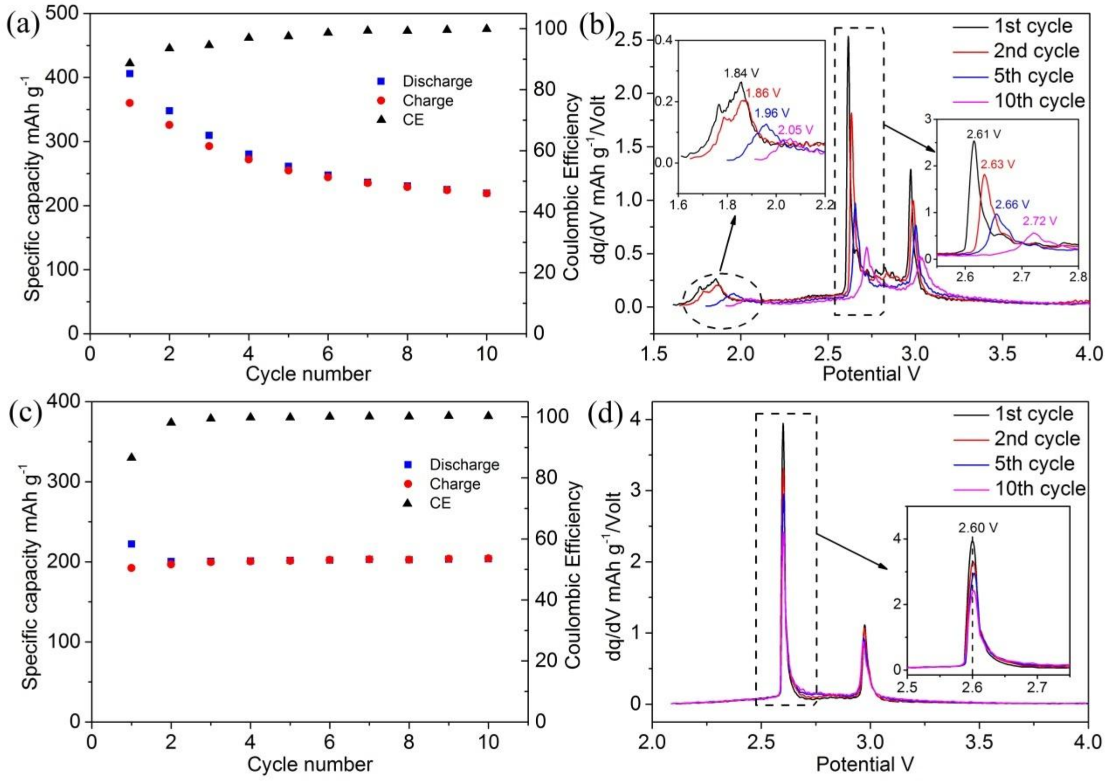

Figure 3. (a, c) The cyclic performance of the $NH_4V_3O_8$ micro/nanoplates cathodes at 50 mA g^{-1} in 1.5-4 V and 2-4 V, respectively. (b, d) The derivative of the voltage-capacity curves in 1.5-4 V and 2-4 V, respectively.

The discharge capacity of the $NH_4V_3O_8$ micro/nanoplates is evaluated at the current density of 50 mA g^{-1} in 1.5-4 V. The initial specific capacity is as high as 406.1 mA h g^{-1} (Fig. 3a), which is higher than recently reported 328 mAh g^{-1} at 15 mA g^{-1} for $NH_4V_3O_8$ nanobelts[13], 210 mAh g^{-1} at 30 mA g^{-1} for $NH_4V_4O_{10}$ nanowires[14], and 265 mAh g^{-1} at 50 mA g^{-1} for $NH_4V_4O_{10}$ powders [20]. This result also exhibit the highest discharge capacity for pure $NH_4V_3O_8$ to the best of our knowledge. In the 10th cycle, the specific capacity dramatically decreased to 219.4 mAh g^{-1}. The derivative of the voltage-capacity curves is applied to illuminate the redox process with Li ion intercalation-deintercalation. As shown in Fig. 3b, on oxidation, three peaks are observed around 1.8 V, 2.6 V and 3.0 V, indicating three steps of the intercalation of lithium ion. It is known that the changes in peak shape, intensity and position can be attributed to kinetic origin. As shown in Fig. 3b insert, the maximum intensity of peaks shifts to a higher voltage, from 2.61 V in 1st cycle, to 2.63 V in 2nd cycle, 2.66 V in 5th cycle and 2.72 V in 10th. The positive shift of the peak position means the increase of polarization of the electrode, which make the Li ions intercalation and de-intercalation more difficult[21]. At the same time, the peak shapes also change greatly. The peak broadening may often be related to the grain size effect in the electrode active material, suggesting that $NH_4V_3O_8$ micro/nanoplates upon cycling would result in an amorphous state. The peaks around 1.8 V show the same trends: the intense positive shift and peak shape broadening, which could be attributed to the increased polarization and amorphization of the electrodes. In the cutoff potential of 2-4 V, the initial specific capacity is 222.1 mAh g^{-1} (Fig. 3c), which is lower than that in 1.5-4 V. However, after 10 cycles, the specific capacity is 203.7 mA h g^{-1}. The capacity retention is up to 91.7% with better cycling stability, which is higher than 54.0% in 1.5-4 V. The derivative of the voltage-capacity curves are shown in Fig. 3d. Two peaks are observed around 2.6 V and 3.0 V, indicating two steps of the intercalation of lithium ion in 2-4 V. The maximum intensity of peaks at 2.6 V, as shown in Fig. 3d insert, shows no positive or negative shift on position; the shape of the peaks almost remain the same. Obviously, without the insertion site at 1.8 V, $NH_4V_3O_8$ electrodes avoid experiencing strong polarization and amorphization. The reaction kinetics are not altered upon cycling, resulting in better cycling performance for $NH_4V_3O_8$ electrodes in 2-4 V.

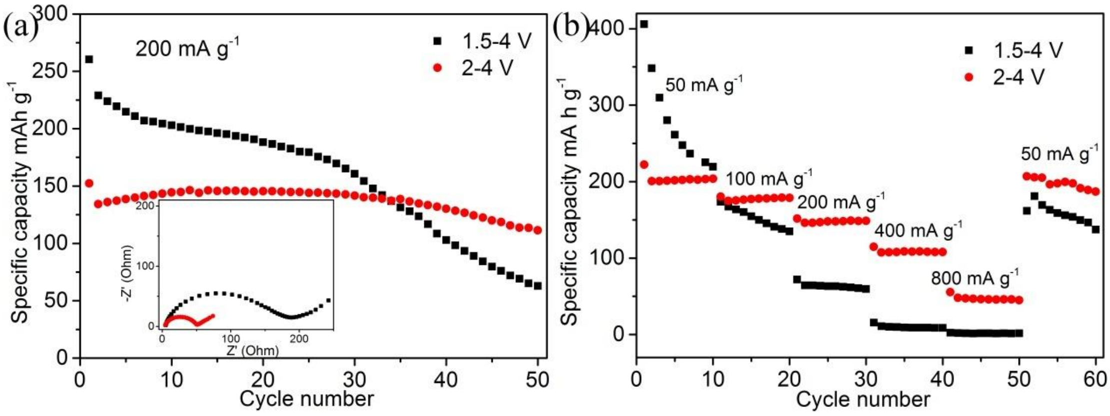

Figure 4. (a) The cyclic performance of the $NH_4V_3O_8$ micro/nanoplates cathodes at 200 mA g^{-1} and (inset) EIS spectra after discharge-charge for three times. (b) Different rate capacity using 1.5-4 and 2-4 V cutoff potentials, respectively.

The discharge capacity of the $NH_4V_3O_8$ micro/nanoplates cathodes is further evaluated at the higher current density of 200 mA g^{-1} (Fig. 4a). In the cutoff potential of 1.5-4 V, the initial specific capacity is up to 260.3 mA h g^{-1}. However, at the 50th cycle, the specific capacity decreased to 62.8 mAh g^{-1}, and the capacity retention is only 24.1%. For comparison, in the cutoff potential of 2-4 V, the initial specific capacity is 152.3 mAh g^{-1}, which is lower than that of 1.5-4 V. However, after 50 cycles, the specific capacity is still 111.5 mA h g^{-1}. The capacity retention is up to 73.2% with better cycling stability, which is three times higher than that of 1.5-4 V. The electrochemical impedance spectroscopy (EIS) measurements are further performed to elucidate the difference in the above cutoff potentials. The Nyquist plots after discharge-charge for three cycles at a current density of 200 mA g^{-1} are shown in Fig. 4a insert. Both electrodes display an arc/semicircle at high-medium frequency and an inclined line at low frequency, which corresponds to charge transfer and diffusion solid-state diffusion process of lithium ions, respectively. The diameter of the semicircle could give an approximate value of the charge transfer resistance: 190 Ω for the electrodes cycled in 1.5-4 V and 51 Ω in 2-4 V. The lower charge transfer resistance in 2-4 V indicate faster kinetics for Li ion insertion/extraction [22].

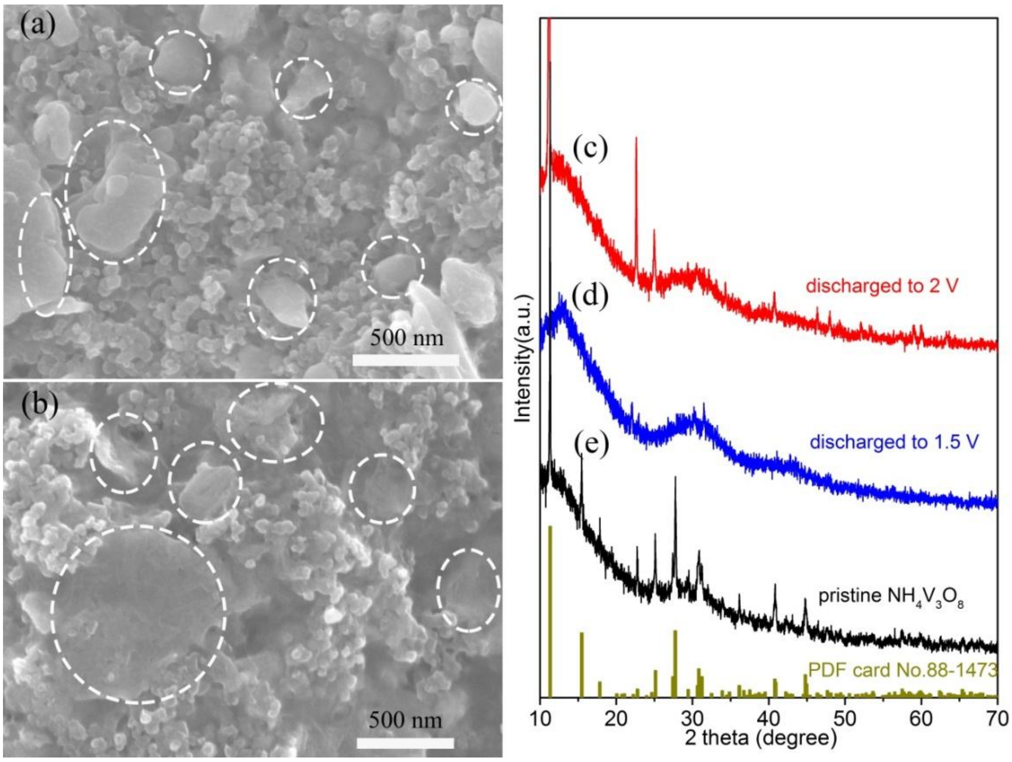

Figure 5. (a, c) SEM images and XRD patterns of electrodes comprising $NH_4V_3O_8$ micro/nanoplates, extracted from cells, discharged to 2 V; (b, d) discharged to 1.5 V at the 3rd cycle. (e) XRD patterns of the pristine $NH_4V_3O_8$ micro/nanoplates.

Rate performance of $NH_4V_3O_8$ micro/nanoplates cathodes in the range of 2-4 V and 1.5-4 V are also compared at different current density ranging from 50, 100, 200, 400 and 800 mA g^{-1}. The discharge capacity measured at every 10th cycle is shown in Fig. 4b. At 50 mA g^{-1}, the average discharge capacity is 204 mAh g^{-1} in the range of 2-4 V, higher than 170 mAh g^{-1} in 1.5-4 V. Further increasing the current density to 100 mA g^{-1}, the value is 177 mA h g^{-1} (vs. 66 mA h g^{-1} in 1.5-4 V). The trend is continued up and the value is further reduced to 148 mA h g^{-1} (vs. 17 mA h g^{-1} in 1.5-4 V) at 200 mA g^{-1}. Even at the current density of 400 and 800 mA g^{-1}, the discharge capacity retention can still be up to 108 and 47 mA h g^{-1}, while the latter one in 1.5-4V shows nearly no discharge capacity. After testing at different current densities, 97% of the original capacity (197 mA h g^{-1}) is recovered when coming back to 50mA g^{-1} in 2-4 V, while the recovery ratio in 1.5-4 V is only 38% (65 mA h g^{-1}). Obviously, the $NH_4V_3O_8$ electrodes presented the higher and more stable cycling and rate performance in 2-4 V than 1.5-4 V.

To investigate the origin of the different performance in the accelerated capacity fading between 1.5 V and 2 V cutoff potentials, we examined SEM images and crystal structures after discharge-charge. When the electrode is discharged to 2 V at the 3rd cycles, the well-shaped $NH_4V_3O_8$ micro/nanoplates (the region in the dotted circle) dispersed among acetylene black can be clearly observed from the SEM image (Fig. 5a). As shown in Fig. 5c, the XRD patterns of cathodes discharged to 2 V show the strong peaks of monoclinic phased $NH_4V_3O_8$. The overall structural framework is therefore preserved through discharge-charge; no indication of significant structural degradation is noted compared to the pristine micro/nanoplates in Fig. 5e. When discharged to 1.5 V, $NH_4V_3O_8$ samples do not retain the original micro/nanoplates morphology as shown in Fig. 5b. This result confirms that the crystal structure transition during cycling make the micro/nanoplates break down into smaller pieces with crimped surfaces. Meanwhile, the XRD patterns in Fig. 5d do not show any obvious diffraction peaks corresponding to $NH_4V_3O_8$. These peaks can hardly be distinguished from the background, indicating a transition from crystal $NH_4V_3O_8$ to an amorphous state after repetitive electrochemical lithiation and delithiation. The poor capacity retention of $NH_4V_3O_8$ discharged to 1.5 V is probably ascribed to the irreversible formation of lithiated phase and vanadium dissolution in the electrolyte[23, 24]. From the above results, we can conclude that the deep lithium ion insertion/deinsertion cause the layered structure disorder/destruction, in accordance with amorphization of the $NH_4V_3O_8$ micro/nanoplates and then capacity fading.

4. CONCLUSIONS

In summary, $NH_4V_3O_8$ micro/nanoplates composed of high crystallined nanosheets are successfully synthesized using a hydrothermal method without any surfactant. Owing to their unique microscopic crystal structure and macroscopic 2D architectures, the $NH_4V_3O_8$ cathodes exhibit very high initial discharge capacities of 406 mAh g^{-1}. To further improve the cyclability, two different cutoff potentials of 1.5-4 V and 2-4 V are investigated. It is found that in a deeper lithium ion intercalation at 1.8 V causes the layered structure of $NH_4V_3O_8$ cathodes disorder/destruction accompanied with strong polarization and amorphization. The suitable cutoff potential of 2-4V can efficiently improve the cycling and rate performance of $NH_4V_3O_8$ cathodes for lithium ion batteries, owing to the stable reaction kinetics for Li ions intercalation.

ACKNOWLEDGEMENTS
This research is supported by NSFC (51402129), China Postdoctoral Science Foundation (2016M601731, 2016M591775), Natural Science Fund project in Jiangsu Province (BK20160529), University Natural Science Research Project of Jiangsu Province (14KJB580004), Research Funds for Senior Professionals of Jiangsu University (13JDG073), Priority Academic Program Development of Jiangsu Higher Education Institutions (PAPD).

References

1. B. Scrosati and J. Garche, *J. Power Sources*, 195 (2010), 2419.
2. D. Liu and G. Cao, *Energy & Environ. Sci.*, 3 (2010), 1218.
3. C. Zhang, Z. Chen, Z. Guo and X. W. Lou, *Energy & Environ. Sci.*, 6 (2013), 974.
4. D. Chao, C. Zhu, X. Xia, J. Liu, X. Zhang, J. Wang, P. Liang, J. Lin, H. Zhang, Z. X. Shen and H. J. Fan, *Nano lett.*, 15 (2015), 565.
5. N. Ding, X. Feng, S. Liu, J. Xu, X. Fang, I. Lieberwirth and C. Chen, *Electrochem. Commun.*, 11 (2009), 538.
6. C. V. Subba Reddy, A. P. Jin, X. Han, Q. Y. Zhu, L. Q. Mai and W. Chen, *Electrochem. Commun.*, 8 (2006), 279.
7. H. Wang, Y. Zeng, K. Huang, S. Liu and L. Chen, *Electrochim. Acta*, 52 (2007), 5102.
8. Y. Xu, X. Han, L. Zheng, S. Wei and Y. Xie, *Dalton T.*, 40 (2011), 10751.
9. G. S. Zakharova, C. Taeschner, T. Kolb, C. Jaehne, A. Leonhardt, B. Buechner and R. Klingeler, *Dalton T.*, 42 (2013), 4897.
10. H. Wang, K. Huang, Y. Ren, X. Huang, S. Liu and W. Wang, *J. Power Sources*, 196 (2011), 9786.
11. H. Wang, Y. Ren, W. Wang, X. Huang, K. Huang, Y. Wang and S. Liu, *J. Power Sources*, 199 (2012), 315.
12. H. Wang, K. Huang, S. Liu, C. Huang, W. Wang and Y. Ren, *J. Power Sources*, 196 (2011), 788.
13. Y. Cheng, J. Huang, J. Li, L. Cao, Z. Xu, J. Wu, S. Cao and H. Hu, *Electrochim. Acta*, 212 (2016), 217.
14. D. Fang, Y. Cao, R. Liu, W. Xu, S. Liu, Z. Luo, C. Liang, X. Liu and C. Xiong, *Appl. Surf. Sci.*, 360 (2016), 658.
15. L. S. Zhong, J. S. Hu, A. M. Cao, Q. Liu, W. G. Song and L. J. Wan, *Chem. Mater.*, 19 (2007), 1648.
16. C. Nethravathi, C. R. Rajamathi, M. Rajamathi, U. K. Gautam, X. Wang, D. Golberg and Y. Bando, *ACS Appl. Mater. Inter.*, 5 (2013), 2708.
17. L. Hu, H. Zhong, X. Zheng, Y. Huang, P. Zhang and Q. Chen, *Sci. Rep.*, 2 (2012), 986.
18. H. L. Fei, M. Liu, H. J. Zhou, P. C. Sun, D. T. Ding and T. H. Chen, *Solid State Sci.*, 11 (2009), 102.
19. G. S. Zakharova, V. L. Volkov, C. Täschner, I. Hellmann, A. Leonhardt, R. Klingeler and B. Büchner, *Solid State Commun.*, 149 (2009), 814.
20. S. Sarkar, P. S. Veluri and S. Mitra, *Electrochim. Acta*, 132 (2014) 448.
21. M. Dubarry, B. Y. Liaw, M. S. Chen, S. S. Chyan, K. C. Han, W. T. Sie and S. H. Wu, *J. Power Sources*, 196 (2011), 3420.
22. Y. Wu, Z. Wen and J. Li, *Adv. Mater.*, 23 (2011), 1126.
23. C. Delmas, S. Brèthes and M. Ménétrier, *J. Power Sources*, 34 (1991) 113.
24. L. Mai, L. Xu, C. Han, X. Xu, Y. Luo, S. Zhao and Y. Zhao, *Nano lett.*, 10 (2010) 4750.